RSC Advances

This is an *Accepted Manuscript*, which has been through the Royal Society of Chemistry peer review process and has been accepted for publication.

Accepted Manuscripts are published online shortly after acceptance, before technical editing, formatting and proof reading. Using this free service, authors can make their results available to the community, in citable form, before we publish the edited article. This *Accepted Manuscript* will be replaced by the edited, formatted and paginated article as soon as this is available.

You can find more information about *Accepted Manuscripts* in the Information for Authors.

Please note that technical editing may introduce minor changes to the text and/or graphics, which may alter content. The journal's standard Terms & Conditions and the Ethical guidelines still apply. In no event shall the Royal Society of Chemistry be held responsible for any errors or omissions in this *Accepted Manuscript* or any consequences arising from the use of any information it contains.

ROYAL SOCIETY OF CHEMISTRY

www.rsc.org/advances

Graphic for manuscript

Manuscript title:

Nanoparticle attachment on nanorings nanoantenna for large increases of Surface-enhanced Raman scattering

Authors:

Zao Yi, Jiangshan Luo, Yong Yi, Xibin Xu, Pinghui Wu, Xiaodong Jiang, Yougen Yi, Yongjian Tang

Table of contents Image:

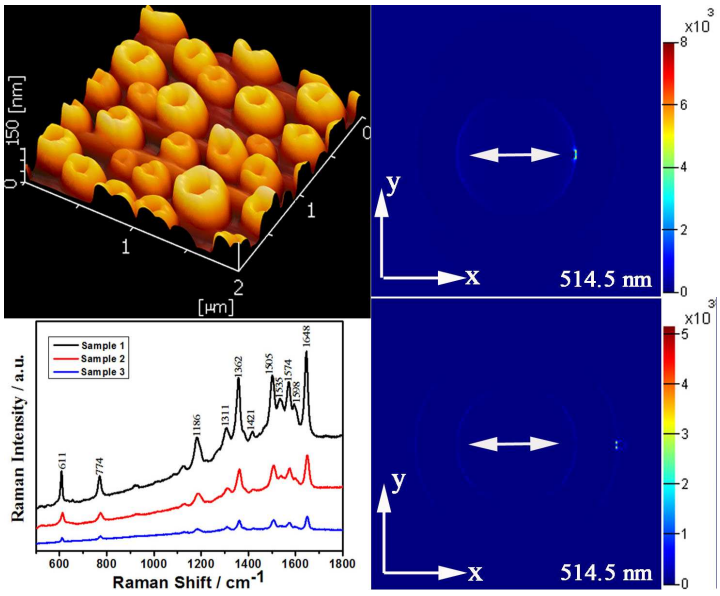

RSC Advances Accepted Manuscript

Nanoparticle attachment on Ag nanorings nanoantenna for large increases of Surface-enhanced Raman scattering

Zao Yi [a,b], Jiangshan Luo [b], Yong Yi[c], Xibin Xu [a,b], Pinghui Wu[d], Xiaodong Jiang [b], Yougen Yi [a*], Yongjian Tang [b**]

[a] *College of Physics and Electronics, Central South University, Changsha 410083, Hunan, China*

[b] *Research Center of Laser Fusion, China Academy of Engineering Physics (CAEP), Mianyang 621900, Sichuan, China*

[c] *Joint Laboratory for Extreme Conditions Matter Properties, Southwest University of Science and Technology and Research Center of Laser Fusion, CAEP, Mianyang 621900, Sichuan, China*

[d] *State Key Laboratory of Modern Optical Instrumentation, Department of Optical Engineering, Zhejiang University, Hangzhou 310027, Zhejiang, China*

***Corresponding author: (Yougen Yi)**

Email: yougenyi@mail.csu.edu.cn

TEL : +86 0816 2480827

FAX: +86 0816 2480830

****Corresponding author: (Yongjian Tang)**

Email: myyz1984@ mail.csu.edu.cn

TEL : +86 0816 2480827

FAX: +86 0816 2480830.

RSC Advances Accepted Manuscript

A simple and inexpensive approach based on heat-treatment of Ag^+/PVA/PVP composite film on quartz glass has been developed for fabricating large-area Ag nanorings attached small nanoparticles. The explosive decomposition of $AgNO_3$, PVA and PVP by calcinations could explain their formation. A maximum enhancement factor of 1.9×10^{10} can be obtained with the self-organized Ag nanorings attached small nanoparticles. Moreover, using the three-dimensional finite-difference time-domain (3D-FDTD) simulations, we provide that the EF can be obviously improved via some small Ag particles attachment on these nanorings because of the strong coupling between the discrete plasmon states of small nanoparticles and the term of propagating plasmons of Ag nanorings. Understanding and realization the enhancing mechanism of nanostructured surfaces attachment small nanoparticles could open potentialities to effectively improve the SERS property of the SERS substrates.

Keywords: Ag nanorings; Small Ag nanoparticle; SERS; 3D-FDTD

1. Introduction

In 1974, Fleischman et al have first observed surface enhanced Raman scattering (SERS) [1]. After that, based on this important technique for trace molecular analysis, many fundamental researches and practical applications have been extensive studied [2-4]. Two mechanisms are often put forward in previous paper to explain the SERS characteristics. The first one is the electromagnetic mechanism (EM), and the second one is the chemical mechanism (CM). The EM mechanism is responsible for the major of SERS enhancement that could give up to 10^{12} enhancement. However, the CM mechanism is considered to be usually in the range of 10-100 [5]. These "hot spots" on the metal surfaces play important role which are regions with a high intensity of an EM field in the enhancement mechanism of SERS [6, 7]. "Hot spots" can be obtained at the adjacent site between metallic nanoparticles or at locality outside of sharp surface protrusion, such as in the gap of aggregated colloids [8], at junctions of

RSC Advances Accepted Manuscript

fabricated nanostructures [9], as well as on the apexes of metallic tips [10]. Thus, preparing substrates with lots of "hot spots" is one of the most important tasks in this field.

Metal nanoring structures are specifically attractive because these structures can induce strong local electric field owing to plasmons forcefully coupled at the interior and exterior surfaces [11, 12]. Moreover, through changing the size and width of the ring, the nanoring exhibits strongly tunable plasmonic resonance from the visible to near-infrared (NIR) region [13]. These properties of nanoring have been used in applications which including optical antennas [14], plasmonic waveguide [15], optical confinement [16], data storage [17] and SERS [18-20]. A variety of methods have been reported to fabricate metal nanorings that including lithography [21, 22], molecular-beam epitaxy [23] and template techniques [24, 25]. Generally speaking, template methods seem to be important for the make of such interesting nanoparticles, no matter what various post treatment are used. And these templates are including polystyrene (PS) nanospheres [26], mesoporous membrane [27], DNA condensates [28] and porous anodic aluminum oxide [29]. However, because technical or economic perspectives, most of these techniques needed either involved complicated procedures or sophisticated instruments which could be limited for large scale production of rings. A functional, reproducible, and low cost nanoring structure SERS active substrate is demanded to enable Raman measurements of various analytes for sensing applications.

Here, in this paper, we provide a convenient and low cost way for the large-area self-organized synthesis of Ag nanorings attached small nanoparticles through heat treatment of Ag^+/PVA/PVP composite film on quartz glass. Because of templates and sophisticated apparatus are not necessary, the way provided here can be an important complement to existing methods for the fabrication of rings. In addition, the as-prepared special structural features with nanoparticle-attached Ag nanorings have been

RSC Advances Accepted Manuscript

applied in SERS properties with Rhodamine 6G (R6G) and 4-aminothiophenol (4-ATP) as the probe molecules. Using the three-dimensional finite-difference time-domain (3D-FDTD) simulation, the theoretical examination of the local EM properties lets us to evaluate the contributions of nanoring and nanoparticle-attached Ag nanorings to the experimentally obtained SERS intensities. Via simulations, we provide that the weak enhancement can be remarkably improved through nanoparticle-attached Ag nanorings and availably utilizing transversely polarized light. In addition to we provide strong lateral coupling induced at the adjacent site between small Ag nanoparticles and nanoring.

2. Experimental details

In the experiment, at first, we prepared an aqueous mixture containing 50 ml of $AgNO_3$, 50 ml of poly-(vinylpyrrolidone) (PVP) and 50ml of poly (vinyl alcohol) (PVA). The mole ratio of PVA, PVP and $AgNO_3$ were tuned from 4:1:3, pass 4:1:4 and 4:1:5, to 4:1:6. Secondly, we spin-coated the mixture at 3000 rpm for 3 min on quartz glass wafer. The number of spin coats is one, two and three, respectively. And then we dried these films in a vacuum overnight. Thirdly, we reduced prepared Ag^+/PVA/PVP film by aqueous H_2O_2, or calcined Ag^+/PVA/PVP film without reduction. In the former experiment, we immersed the prepared Ag^+/PVA/PVP film into 10 mM aqueous H_2O_2 for 10 min. And then the film was rinsed with deionized water, dried in vacuum overnight finally. At last, we calcined these spin coated films at a rate of 2℃/min from room temperature to 700℃. In this process, we kept at 700℃ for 4 hours under Ar gas ambience. And finally we allowed these films to cool.

In SERS spectra measurements, first of all, by using an accurate pipette, we dropped a 10 μL droplet of 1.0×10^{-6} mol/L ethanol solution of 4-aminothiophenol (4-ATP) or 1.0×10^{-6} mol/l aqueous solution of rhodamine 6G (R6G). Secondly, let the samples dried in air at ambient temperature, in order to gain a uniform molecule membrane over an area of about 10 mm^2. In this experiment, we prepared

RSC Advances Accepted Manuscript

three samples with the same about SERS-active substrates. In addition, each sample was used to select ten different points in order to detect the 4-ATP or R6G probes which confirm the reproducibility and stability of these samples. We used Renishaw 2000 model confocal microscopy Raman spectrometer which includes a CCD detector and a holographic notch filter to measure SERS spectra. Leica DMLM system was adopted in the microscope attachment. The laser beam was focused onto a spot about 1 μm in diameter by using a 100×objective. The SERS was excited by using radiation of 514.5 nm that from an air-cooled argon ion laser which was about 7.2 mW at the position of samples. The recorded time of the Raman spectra is 20 s.

3. Simulation methods

We used a commercial FDTD calculation for 3D-FDTD simulations [30]. The boundary conditions of the simulation domain are perfectly matched layer absorbing boundaries. The calculation region is 0.8 × 0.8 × 0.2 μm^3, and the cell size is 1 × 1 ×1 nm^3. We installed propagation directions of plane waves parallel with the x axis. In order to closely match the experimental condition, the model of Ag nanostructures was introduced. The Fig. 1 shows the schematic geometries of the structures studied. The scheme of Ag nanoring with outer radius r_1 (r_1 = 250 nm), inner radius r_2 (r_2 = 150 nm) and thickness h (h = 100 nm) is shown in Fig. 1 (a). The scheme of Ag nanosphere with radius r (r = 250 nm) is shown in Fig. 1 (b). The Fig. 1(c-d) shows these models of Ag nanoring attached one small Ag nanoparticle with different site: (c) interior surface; (d) exterior surface. We set the simulation time to be 300 fs, and input pulse width is 14.70 fs in order to ensure the fields decay completely. In our simulation, the dielectric function of Ag nanostructure was described by the Lorenz-Drude model [31]. The refractive index of surrounding medium was set to be 1.0 for air and the dispersion of quartz glass substrate was considered. The dielectric constants of the glass have been taken from Palik [32]. We

RSC Advances Accepted Manuscript

express the near-field intensity enhancement images. They are set up by dividing the electric field strength ($E^2 = Ex^2 + Ey^2 + Ez^{2)}$ around the Ag nanostructure. In the simulation, first of all, we calculate the local electric field. And then evaluate the field intensity for each mesh through integration. At last we compare the computation with the EF values which come from the measured Raman spectra.

4. Results and discussion

On the basis of the heat treatment of Ag^+/PVA/PVP composite film on quartz glass wafer, we can obtain large-area self-organized Ag nanorings attached small nanoparticles. During the high temperature, the organic components are removed, and $AgNO_3$ is decomposed into Ag^0, and released nitrogen, oxygen, and nitrogen oxides. These Ag^0 produced were unstable and could aggregate to form Ag clusters. The SiO_2 layer of quartz glass wafer forcefully interacts with Ag^0 and will decrease the activity of Ag^0. The activity of Ag^0 can be decreased with aggregation and then particle size is increased. Through the strong bonding interaction between the outmost orbital of Ag nanoparticle surface atoms and the contacting oxygen atoms of quartz glass wafer, these metal nanoparticles will be stabilized [33, 34]. The morphologies can be controlled by the experiment condition. The Fig. 2 shows the images of the Ag nanorings attached small nanoparticles. The Ag^+/PVA/PVP film is two layers. The mole ratio of PVA, PVP and $AgNO_3$ is 4:1:4. Self-organized Ag nanorings attached small nanoparticles were formed when the as-prepared Ag^+/PVA/PVP film was subjected to calcinations without reduction. The low magnification SEM image (in Fig. 2A) obviously shows homogenously distributed self-organized Ag nanorings attached small nanoparticles covering large areas. In Fig. 2B, the high magnification SEM image shows the products are all ring shape with average outer diameter (~500 nm) and inner diameter (~300 nm). Very interestingly, lots of small nanoparticles of average 20 nm in diameter are observed around the Ag ring, which are expected to provide lots of “hot spots” for

RSC Advances Accepted Manuscript

chemical catalysis. The reason is that the distribution of the small Ag seeds is not homogeneous on the substrate surface at the beginning of the heat treatment. Because closing enough these small nanoparticles will collide and fuse with each other via thermal treatment. Then these small nanoparticles form a larger nanoparticle, so as to leave a blank area surrounding it. On the contrary, these nanoparticles would stay intact when are located far enough. Fig. 2C and D show tilted-view (ca. 15°) SEM images of the self-organized Ag nanorings arrays. Through atomic force microscopy (tapping mode), the structure of Ag nanorings was further confirmed (as shown in Fig. 3.) The Fig. 3A represents that these products are all nanoring shape, which is consistent with the SEM study (as shown the Fig 2). The deep color in the nanoring is the hole of the nanoring. The Fig. 3B gives the 3 D image of the Ag nanorings. The image confirms the Ag nanorings with an average thickness of 100~150 nm. The detailed morphology analyses have been reported in our previous paper [35].

PVA and PVP are well known organic polymers and are mostly used as a water soluble organic binder. In the past several years, as a template and a capping agent for nanoparticles synthesize, the PVA and PVP have been used widely [36, 37]. In our study, the mole ratio between PVA, PVP and $AgNO_3$ can control the shape of Ag nanoparticles. As shown the Fig 4, two types of morphology of Ag nanoparticles that one is nanoring, and the other is hemispherical or spherical are obvious on the surface of quartz glass wafer. Fig. 4A corresponding to the mole ratio of 4:1:3 (sample 2) represents lots of monodisperse Ag nanorings cover the quartz glass wafer surface. Compared the nanorings prepared with the mole ratio of 4:1:4, as shown the Fig. 4B, the average size (the Fig. 4A) is much small that outer diameter is 300 nm and inner diameter is 120 nm. However, as shown the Fig. 4C, lots of Ag nanoparticles with inhomogeneous size appear on the quartz glass wafer surface when the $AgNO_3$ concentration rises to 4:1:5 (sample 3). The shape of nanoparticles is all hemispherical and

RSC Advances Accepted Manuscript

spherical. While in Fig. 4D, no nanorings can be found but the particles with bigger size, corresponding to the mole ratio of 4:1:6 (sample 4). The diameter of particles and ratio of big size particles increase dramatically when the $AgNO_3$ concentration increases. The SEM research represents that the Ag products experience the evolution of size and morphology that the size changes from small to big and the morphology changes from nanoring to nanosphere. In a word, the mole ratio of PVA, PVP and $AgNO_3$ plays a significant role in our study. The reason is that it determines the distance of the Ag particles and clusters, by which particles and clusters will aggregate via different mode. If the $AgNO_3$ concentration is very high, due to the close distance, these Ag nanoparticles and nanoclusters could aggregate to each other, so as to form a hemispherical or spherical morphology easily. However, if the $AgNO_3$ concentration is very low, due to the relatively long distance, these Ag nanoparticles and nanoclusters could aggregate to be low dome morphology. As the annealing process goes on, as shown the Fig. 4C and D, these hemispherical and spherical shaped Ag aggregates will grow to metallic Ag without any change in their morphology. However, these dome shaped Ag aggregates contain many unreleased organic composites and HNO_3. As shown the Fig. 4A and B, these releasing gaseous CO_2, H_2O and NO_2 will break through the top of the dome when the temperature rise highly enough, so these dome shaped Ag aggregates come into being with ring shapes.

The thickness of the prepared spin coated films can influence the morphology of nanoparticles also. As mentioned in our experiment, these films have different thickness as a result of the different number spin coats. Fig 5 represents the SEM images of the Ag^+/PVA/PVP composite film with different thickness. The SEM images represents that the formation process of ring nanostructure can be controlled by the thickness of film. When the spin coat is one, as expect the shape of nanoparticles is nanoring, as shown the Fig 5A. However, when the spin coat is three, lots of bigger size particles

RSC Advances Accepted Manuscript

prepared and no Ag nanorings can be found, as shown the Fig 5B. It can be seen that these Ag nanoparticles and nanoclusters could aggregate to each other, so as to form a hemispherical or spherical morphology easily, due to the close distance. On the basis of the above experimental results, the optimal spin coat is two coats for the formation of Ag nanoring.

It is useful to speculate on the mechanism of Ag nanorings formation at this experiment. Ag^+/PVA/PVP were composed by PVA and PVP that serve as a binder. The hydroxyl groups of PVA and PVP are ligands to Ag^+. These hydroxyl groups are necessary for homogeneous dispersion of Ag^+. The prepared spin coated films are composed of PVA, PVP and small Ag nanoparticles. At the beginning, the mixing aqueous $AgNO_3$, PVA and PVP are the colorless precursor solution. After stirring for one hour at room temperature, they become deep yellow and then dark later. That means small Ag nanoparticles appear in the mixing aqueous [38]. In order to transform more Ag^+ into Ag^0, we immersed the prepared Ag^+/PVA/PVP film (two layers) on quartz glass wafer into aqueous H_2O_2. And then the film was rinsed with deionized water, dried in vacuum overnight finally. Fig. 6 represents the SEM image of the as-treated film by aqueous H_2O_2. We can see lots of small Ag nanostructures that are reduced by the PVA, PVP distributed on the substrate surface. These small nanoparticles and nanoclusters are embedded in PVA/PVP composite [38]. The large particles are reduced by H_2O_2. The diameter is about 20 nm. The Fig 7 is the 3 D image of nanoparticles on quartz glass wafer with different experiment conditions, which Fig 7A is the heat treatment of Ag^+/PVA/PVP composite film after reduction by H_2O_2, Fig 7B is the heat treatment of Ag^+/PVA composite film without reduction and Fig 7C is the heat treatment of Ag^+/PVA/PVP composite film without reduction. These films are two layers. When the Ag^+/PVA/PVP composite film was reduced by H_2O_2, lots of large particles (~20nm) appeared, as shown the Fig. 6. From Fig 7A, these large silver aggregates grow to

RSC Advances Accepted Manuscript

hemispherical and spherical silver nanoparticles without any change in the morphology. The 3 D image of the Ag nanoparticles confirms the hemispherical and spherical Ag nanoparticles with an average thickness of 150~200 nm. The SEM image these Ag nanoparticles prepared after reduction by H_2O_2 is shown in Fig. S1. The average diameter is about 500 nm. As we known, the decomposition peak of PVA is at approximately 300℃ in the derivative TGA curve [39]. And the decomposition peak of PVP is at approximately 380℃ in the derivative TGA curve [40]. In our experiment, through the different decomposition temperature of the PVA and PVP, we could get the Ag nanorings on quartz glass wafer. Fig. 8 shows the TGA thermogram of the Ag^+/PVA/PVP composite film. The mole ratio of PVA, PVP and $AgNO_3$ is 4:1:4. The thermogram was collected in Ar gas atmosphere (200 ml min^{-1}) from 50 °C to 1000 °C, under a heating rate of 10 °C min^{-1}. PVA chains are going to change to crosslink after high temperature (250℃) treatment when the annealing process begins. PVA will be decomposed and removed when the temperature rises to 300℃. These Ag^+/PVA particles which contain NO_3^- and PVA molecules will decompose, and then release gaseous N_2, O_2, CO_2, H_2O, and nitrogen oxides via thermal treatment. During in the process, because of gas release, the large Ag^+/PVA particles probably expand via thermal treatment to collapse, and later to metal nanoring. However, as shown the Fig 7B, when the heat treatment film is the Ag^+/PVA composite film, the production are not all nanoring. And these nanorings do not exhibit distinctness. The AFM images and the section analysis obtained by AFM are shown in Fig. S2. These results are as like the previously reported [34]. When the temperature rise highly enough to 380℃, these PVP molecules in the nanoparticles appear decomposition. Then the releasing CO_2, H_2O and NO_2 gas will break through the top or side of these spherical Ag nanoparticles again, so the nanoparticles come into being with ring shapes, as depicted from Fig 7C. From these contradistinctive experiment, we know that the secondly gas release from the PVP is very important for

RSC Advances Accepted Manuscript

the forming nanoring.

Since Ag nanorings display different electric field characteristic compared Ag spherical nanoparticles, which may lead to large SERS enhancement. To investigate the SERS sensitivity of Ag nanoparticles substrates, the SERS spectra of 4-ATP were measured under the same experimental conditions (laser power = 50 μW, microscope objective = 50×, acquisition time = 20 s) with Raman spectrometer. As shown the Fig. 9, black, red and blue lines correspond to the sample 1, sample 7 and sample 8, respectively. Two kinds of bands were looked on the SERS spectra of 4-ATP on the Ag nanoparticles film. One kind is located at 1073 and 1185 cm^{-1}, which are assigned to the a_1 vibration modes, and the other kind is located at 1143, 1388, 1436, and 1577 cm^{-1}, which are assigned to the b_2 vibration modes [41]. The intensity increase of the b_2 and a_1 modes is associated mainly with the CM and EM effect, respectively [42]. Therefore, the SERS enhancement of our samples comes from both CM and EM effects. Obviously, the EF gets improved when the 4-ATP molecules are absorbed on the Ag nanorings structure (sample 1). We strongly believe that the strong SERS effect on the Ag nanorings structure is caused by two effects. First one is EM mechanism due to the strong coupling of the LSP of the Ag nanorings. The second one is the CM effect that induced the charge transfer (CT) behavior between Ag nanorings and 4-ATP molecules. Because of the inner region of Ag nanorings, the inner region of nanorings can offer suitable active sites for detection of molecular binding. This structure can be considered as the Ag/4-ATP/Ag sandwich structure, the charge transfer model of the "donor-bridge-acceptor" system may be possible to the present structure.

To inquire the enhancement factor (EF) of these structures quantitatively (sample 1, sample 7 and sample 8), here we take R6G as test molecules. Fig. 10 presents the SERS spectrum of R6G with different samples that are sample1, sample 7 and sample 8, the concentration is 1×10^{-6} M. We have

RSC Advances Accepted Manuscript

assigned the spectral traits of R6G in detail previously so we will not repeat here again [43]. As shown, the R6G molecules on hemispherical and spherical Ag nanoparticles film (sample 8) displayed very light signal. However, the R6G molecules on the Ag spherical nanoparticles and nanorings film (sample 7) displayed a medium SERS signal. Compared to the response of the sample 7, the sample 1 (Ag nanorings film) displayed a much stronger SERS response. These different SERS enhancements can been reveal by the comparison of these spectra, especially the quantitative intensity comparison from the band of 1648 cm^{-1}. To determine the enhancement effect (EF) of R6G on the nanoparticles quantitatively [44, 45], the EF values of R6G in the nanoparticles are calculated with the following expression (the detailed calculation could be seen in the Supporting Information):

$$EF = \frac{I_{SERS}}{I_{\mathrm{Re}f}} \bullet \frac{N_{\mathrm{Re}f}}{N_{SERS}}$$

Then the EF for the sample 1, sample 7 and sample 8 were roughly estimated by comparing the peak intensity at 1648 cm^{-1} to 1.9×10^{10}, 2.9×10^{9} and 9.8×10^{8}, respectively. The SERS spectrum of the Ag nanorings film substrate reveals SERS signals about16 times larger than the Ag spherical nanoparticles film substrate. The absorption spectra of Ag nanoparticles on quartz glass wafer with different experiment conditions are shown in Fig. S3. The SERS enhancement probably related to the following factors. First of all, the larger surface area of the Ag ring nanostructures can induce the SERS enhancement (as shown the Fig. 4). Lots of “hot spots” created at the inner of nanorings could be contributors to this increased response also. So as to the strong SERS enhancement can appear to be in the middle of the nanorings, even though these probe molecules are appeared on the nanorings’ interior or exterior surface. Secondly, the strong intense electromagnetic field can be produced in the nanoring structures. The strong field enhancement suggests that the interior surface of Ag nanorings can afford suitable active sites for detection of molecular binding, even for biosensor applications. These

RSC Advances Accepted Manuscript

biomolecules in the surrounding media can be generally accessible to the region inside of the nanorings, unlike in conventional nanoshells. The result can make nanorings advantageous for using in SERS applications [12]. In our case, because of the coupling between the discrete plasmon states of small nanoparticles and the term of propagating plasmons states of nanorings, the SERS enhancement could be further stronger when small nanoparticle attachment on the Ag nanorings. The junction of the small nanoparticles and nanorings can serve as the hot sites.

The 3D-FDTD method was applied to compute the electromagnetic field distribution which surrounds the laser-illuminated Ag nanorings by numerically solving Maxwell's equations, in order to further indicate the physical mechanism of SERS enhancements of the Ag nanorings (as shown in Fig 11). The SERS effect of Ag nanorings could be further improved by attaching small Ag nanoparticle due to lots of "hot spots" formed at the interface between nanoparticles, as shown the SEM image in Fig. 2B. The Fig 11 (A-C) have shown the E-field amplitude patterns from theoretical calculations at the excitation wavelength of 514.5 nm for Ag nanoring attached one small Ag nanoparticle with exterior surface. The diameter of small Ag nanoparticle is 20 nm. When the polarization directions change from 0º to 90º, the maximal electric field strength $(|E|/|E_0|)^2$ (E is the local fields, E_0 is the input fields.) is found to be about 5.2×10^3, 510 and 62 for three models (The color bars of Fig. 11 (A~C). The units are $(V/m)^2$)) , respectively. For SERS, it is widely believed that $|(|E|/|E_0|)|^4$ is the factor for the Raman intensity increases [46]. The maximum SERS enhancements on the three models correspond to 2.7×10^7, 2.6×10^5 and 3.8×10^3, separately. Comparing with the isolated Ag nanoring, the field intensity of Ag nanoring attached one small Ag nanoparticle is much stronger than them (as shown the Fig. 11A), the reason is that Ag nanoring attached nanoparticle mode can make electromagnetic energy successive transfer at the adjacent site, so as to extremely large field concentration. Briefly, the discrete plasmon

RSC Advances Accepted Manuscript

modes of small Ag nanoparticles couple with the term of propagating plasmons modes of Ag nanoring. The virtual states can be created by the coupling between discrete and continuous modes. These surface charges on the adjacent region of the small nanoparticle and nanoring can provide stronger electric field enhancement. Lots of localized discrete plasmon modes can be created by the hybridization between the nanoring and the small Ag nanoparticle[47]. And some of modes can be shifted to the visible or near infrared region. A strong coupling could be appeared when the wavelength of a plasmon mode is in vicinity of the Raman excitation wavelength. As shown the Fig. 11(A~C), when the polarization direction become small, the EF could be increased 3~4 orders of magnitude. When its polarization direction is changed, the localized surface plasmon (LSP) coupling will be newly distributed between the two nanoparticles. The EF enhancement was suppressed by the LSP coupling "delocalization" and "distribution", the reason is that a parallel orientation of LSP coupling, which coupling with polarization, is essential for getting extremely light intensity. Because the tensor mode polarization is the key for nonlinear optical phenomena, this will be more preferable for EF enhancement [48]. Therefore, the polarization of incident light could control the nanoparticles surface plasmonic field distribution clearly. Here, we have study the local electric field distribution of Ag nanoring attached one small Ag nanoparticle with interior surface, as shown the Fig. 11 (D~F). Compared with Ag nanoring attached one small Ag nanoparticle with exterior surface, as shown Fig. 11 (A~C), the maximal electric field strength $(|E|/|E_0|)^2$ is increased with same polarization direction and the diameter of small Ag nanoparticle. For example, as shown the Fig. 11D, the maximal electric field strength $(|E|/|E_0|)^2$ at the junction of particles is about 8.0×10^3 that lager the 5.2×10^3 (Fig. 11A). The reason is that the local electric field distribution of nanoring has many different at interior and exterior surfaces.

RSC Advances Accepted Manuscript

As we known that the local EM enhancement would increase when the particles size increased. However, because of inelastic scattering, these particles would absorb less light and scatter more when particle size increased [49]. So the overall SERS intensity would decrease. Moreover, the total surface area of adsorption would decrease when the amount of nanoparticles was fixed and the size of nanoparticles was increased. This reason would offset the increased EM field for larger particles [50]. Therefore, it is very significant to confirm the optimal size of the attached Ag nanoparticle to solve the balance problem between scattering limited surface area and EM field increase, so as to realize the strongest SERS intensity. Here, for the model four (as shown the Fig. 1 d), we have changed the diameter of attached small Ag nanoparticle from 15 nm to 30 nm only, and the diameter of nanoring was kept. The input light is polarized along the x-axis. As shown the Fig 11 A and Fig 12, the EF of five models increase in a series: 10 nm < 15 nm < 30 nm < 25 nm < 20 nm, on the basis of the 3D-FDTD calculation results of the maximum field enhancement ($(|E|/|E_0|)^2$). According to the connection dynamic depolarization and radiation damping with corresponding to surface scattering, Meier et al. have predicted the optimal diameter of Ag nanoparticles is 25 nm for SERS [51]. However, in our study, the small Ag nanoparticle attached big nanoring could have increased the resultant EM field assuming equal excitation. And the shorter wavelength absorption of smaller nanoparticles could cause a decrease in the excitation of smaller nanoparticles. Therefore, the small Ag nanoparticle (D=20 nm) is likely to be more appropriate for a higher field enhancement. So, the small attached Ag nanoparticle (D=20 nm) can provide the strongest SERS enhancement factor.

5. Conclusions

In summary, large-area self-organized Ag nanorings attached small nanoparticles have been synthesized on quartz glass substrates by a simple and convenient heat treatment approach. The typical

RSC Advances Accepted Manuscript

Ag nanorings attached small nanoparticles were synthesized as following: The molar ratio of PVA, PVP and $AgNO_3$ is 4:1:4, the Ag^+/PVA/PVP composite film does not be reduction, the number of spin coats is two. Via 3D-FDTD simulations, we provide that the weak enhancement can be remarkably improved through nanoparticle-attached Ag nanorings and availably utilizing transversely polarized light. The creation of Ag nanoring attached one small Ag nanoparticle junctions led to a relatively uniform enhancement of 2.7×10^7, over 4 orders of magnitude stronger than that of the Ag nanoring alone. It can be found that the EF of three kinds of Ag nanoring attached one small Ag nanoparticle with different polarization directions increased in a series: 90°<45°<0°. Compared with Ag nanoring attached one small Ag nanoparticle with exterior surface, the maximal electric field strength $(|E|/|E_0|)^2$ of the Ag nanoring attached one small Ag nanoparticle with interior surface is increased with same polarization direction. The small attached Ag nanoparticle (D=20 nm) with the Ag nanoring can provide the strongest SERS enhancement factor. We hope the way can provide helpful guidelines for the development of SERS properties.

Acknowledgments

The work is supported by the National Natural Science Foundation of China (No. 10804101; 60908023; 11375159), Science and Technology Development Foundation of Chinese Academy of Engineering Physics (No. 2010B0401055), Open Foundation of Joint Laboratory for Extreme Conditions Matter Properties, Southwest University of Science and Technology and Research Center of Laser Fusion, CAEP (No. 12zxjk07), Scholarship Award for Excellent Doctoral Student granted by Ministry of Education (1343-76140000014), Hunan Provincial Innovation Foundation for Postgraduate (No. CX2012B114), and the Open-End Fund for the Valuable and Precision Instruments of Central South University (CSUZC2012032).

RSC Advances Accepted Manuscript

Electronic supplementary information

Electronic supplementary information (ESI) available: SEM image, absorption spectrum and AFM images.

References

[1] M. Fleischmann, P. J. Hendra, A. J. McQuillan, *Chem. Phys. Lett.* 1974, 26, 163-166.

[2] S. Nie, S. R. Emory, *Science.* 1997, 275, 1102-1104.

[3] C. Yang, Y. T. Xie, M. M. F. Yuen, X. M. Xiong, C. P. Wong, *Phys. Chem. Chem. Phys.,* 2010,12, 14459-14461.

[4] J. Ando, T. Yano, K. Fujita, S. Kawata, *Phys. Chem. Chem. Phys.,* 2013, 15, 13713-13722.

[5] K. Yasutaka, T. Yuhei, I. Tamitake, O.Yukihiro, *Phys. Chem. Chem. Phys*., 2010, 12, 7457-7460.

[6] S. L. Kleinman, R. R. Frontiera, A. I. Henry, J. A. Dieringer, R. P. Van-Duyne, *Phys. Chem. Chem. Phys.,* 2013,15, 21-36.

[7] L. M. Tong, H. Wei, S. P. Zhang, Z. P. Li, H. X. Xu, *Phys. Chem. Chem. Phys.,* 2013,15, 4100-4109.

[8] S. L. Kleinman, E. Ringe, N. Valley, K. L. Wustholz, E. Phillips, K. A. Scheidt, G. C. Schatz, R. P. Van-Duyne, *J. Am. Chem. Soc*. 2011, 133, 4115-4122.

[9] X. M. Feng, F. X. Ruan, R. J. Hong, J. S. Ye, J. Q. Hu, G. Q. Hu, Z. L.Yang, *Langmuir* 2011, 27, 2204-2210.

[10] P. Brodard, M. Bechelany, L. Philippea, J. Michler, *J. Raman Spectrosc.* 2012, 43, 745-749.

[11] J. Aizpurua, P. Hanarp, D. Sutherland, M. Käll, W. B. Garnett, F. J. GarcíadeAbajo, *Phys. Rev. Lett.* 2003, 90, 057401-057404.

[12] M. L. Elin, A. Joan, K.; Mikael, S. S. Duncan, *Nano Lett.* 2007, 7, 1256-1263.

[13] A. W. Clark, J. M. Cooper, *Small* 2011, 7, 119-125.

RSC Advances Accepted Manuscript

[14] H. M. Gong, L. Zhou, X. R. Su, S. Xiao, S. D. Liu, Q. Q. Wang, *Adv. Funct. Mater.* 2009, 19, 298-303.

[15] K.Y. Jung, F. L. Teixeira, R. M. Reano, *J Lightwave Technol* 2007, 25, 2757-2765.

[16] Y. Babayan, J. M. McMahon, S. Li, S. K. Gray, G. C. Schatz, T. W. Odom, *ACS Nano* 2009, 3, 615-620.

[17] K. P. Chiu, K. F. Lai, D. P. Tsai, *Opt. Express* 2008, 16, 13885-13892.

[18] M. G. Banaee, K. B. Crozier, 2010, *Opt Lett* 35, 760-762.

[19] Y. M. Hou, J. Xu, P. W. Wang, D. P. Yu, *Appl. Phys. Lett.* 96, 2010, 203107-203109.

[20] J. Ye, S. Masahiko, L. Kristof, L. Liesbet, K. Tatsuro, V. Pol, *Appl. Phys. Lett.* 2010, 97, 163106-163108.

[21] N. Rachel, T. Christopher, J. S. Duan, P. Ruth, E. S. Mostafa, *Nano Lett.* 2012, 12, 2158-2164.

[22] G. B. Mohamad, B. C. Kenneth, *ACS Nano,* 2011, 5, 307-314.

[23] F. Q. Sun, J. C. Yu, X. C. Wang, *Chem. Mater.* 2006, 18, 3774-3779.

[24] F. Yan, W. A. Goedel, *Angew Chem Int Ed* 2005, 44, 2084-344.

[25] Y. J. Cai, Y. Li, N. Peter, S. C. Paul, *Nano Lett.* 2012, 12, 4881-4888.

[26] T. A. Kelf, Y. Tanaka, O. Matsuda, E. M. Larsson, D. S. Sutherland, O. B. Wright, *Nano Lett.* 2011, 11, 3893-3898.

[27] F. Yan, W. A. Goedel, *Nano Lett.* 2004, 4, 1193-1196.

[28] J. H. Liu, X. L. Zhang, M. Yu, S. M. Li, J. D. Zhang, *Small,* 2012, 8, 310-316.

[29] S. Zhao, H. Roberge, A. Yelon, T. Veres, *J. Am. Chem. Soc.* 2006, 128, 12352-12353.

[30] The simulations were performed by the FDTD Solutions trademark software. http//: www. lumerical. com.

RSC Advances Accepted Manuscript

[31] A. D. Rakic, A. B. Djurisic, J. M. Elazar, M. L. Majewski, *Appl. Opt.* 1998, 37, 5271-5283.

[32] E. D. Palik, Handbook of optical constants of solids III. Academic, New York. 1998.

[33] J. He, I. Ichinose, T. Kunitake, A. Nakao, Y. Shiraishi, N. Toshima, *J. Am. Chem. Soc.* 2003, 125, 11034-11040.

[34] J. H. He, K. Toyoki, *Langmuir* 2006, 22, 7881-7884.

[35] Z. Yi, X. B. Li, J. S. Luo, Y. Yi, X. B. Xu, P. H. Wu, X. D. Jiang, W. D. Wu, Y. G. Yi, Y. J. Tang, *Plasmonics* DOI 10.1007/s11468-013-9634-7.

[36] K. Subrata, H. David, K. Wang, H. Liang, *J. Colloid Interf. Sci.* 2010, 344, 334-342.

[37] Z. Yi, J. B. Zhang, H. He, X. B. Xu, B. C. Luo, X. B. Li, K. Li, G. Niu, X. L. Tan, J. S. Luo, Y. J. Tang, W. D. Wu, Y. G. Yi, *Trans. Nonferrous Met. Soc. China* 2012, 22, 865-872.

[38] B. Dong, X. Bai, W. Yu, L. Xu, J. S. Chen, D. Li, H. W. Song, *J Mater Sci: Mater Electron.* 2011, 22, 64-71.

[39] N. Gordon, Z. R. Yue, M. Sharifeh, M. Eric, E. James, *Nanotechnology* 2009, 20 495705.

[40] Y. K. Du, P. Yang, Z. G. Mou, N. P. Hua, L. Jiang, *Journal of applied polymer.* 2006, 99, 23-26.

[41] L. L. Sun, Y. H. Song, L. Wang, C. L. Guo, Y. J. Sun, Z. L. Liu, Z. Li, *J. Phys. Chem. C* 2008, 112, 1415-1422.

[42] X. G. Hu, T. Wang, L. Wang, S. J. Dong, *J. Phys. Chem. C* 2007, 111, 6962-6969.

[43] Z. Yi, S. Chen, Y. Chen, J. S. Luo, W. D. Wu, Y. G. Yi, Y. J. Tang, *Thin Solid Films* 2012, 520, 2701-2707.

[44] Z. Yi, X. B. Xu, X. B. Li, J. S. Luo, W. D. Wu, Y. J. Tang, Y. G. Yi, *Appl. Surf. Sci.* 2011, 258, 212-217.

[45] Z. Yi, X. L. Tan, G. Niu, X. B. Xu, X. B. Li, X. Ye, J. S. Luo, B. C. Luo, W. D. Wu, Y. J. Tang, Y.

RSC Advances Accepted Manuscript

G. Yi, *Appl. Surf. Sci.* 2012, 258, 5429-5437.

[46] P. Dawson, J. A. Duenas, M. G. Boyle, M. D. Doherty, S. E. J. Bell, *Nano Lett.* 2011, 11, 365-371.

[47] Y. S. Hu, J. Jeon, T. J. Seok, S. Lee, J. H. Hafner, R. A. Drezek, H. Choo, *ACS Nano* 2010, 4, 5721-5730.

[48] P. N. Prasad, D. J. Williams, Wiley-Interscience: New York, 1991.

[49] K. L. Kelly, E. Coronado, L. L. Zhao, G. C. Schatz, *J Phys Chem B* 2003, 107, 668-677.

[50] G. S. Kevin, C. S. Juan, *J. Phys. Chem. C* 2011, 115, 1403-1409.

[51] M. Meier, A. Wokaun, *Opt. Lett.* 1983, 8, 581-583.

RSC Advances Accepted Manuscript

Figure captions:

Fig 1 (a)The model of the Ag nanoring; (b) the model of the Ag nanosphere; (c) the model of Ag nanoring attached one small Ag nanoparticle with interior surface; (d) the model of Ag nanoring attached one small Ag nanoparticle with exterior surface.

Fig 2 [(A) and (B)]Typical top-view SEM images of Ag nanorings (sample 1) on quartz glass wafer [35], [(C) and (D)] tilted-view (ca. 15°) SEM images of Ag nanorings on quartz glass wafer.

Fig 3 AFM and 3-Dimensional image of Ag nanorings (sample 1) on quartz glass wafer.

Fig 4 SEM images of the Ag nanoparticles obtained from different mole ratio of PVA, PVP and $AgNO_3$. A, B, C and D are corresponding to the mole ratio of 4:1:3 (sample 2), 4:1:4 (sample 1), 4:1:5 (sample 3) and 4:1:6 (sample 4), respectively. The inset images are the magnified SEM images of the corresponding samples.

Fig 5 SEM of silver nanoparticles prepared by different spin coats: (A) one coat (sample 5); (B) three coats (sample 6). The mole ratio of PVA, PVP and $AgNO_3$ is 4:1:4. The inset images are the magnified SEM images of the corresponding samples.

Fig 6 SEM image of the Ag/PVA/PVP film (two layers) after reduction by H_2O_2, where solid and doted arrows point to small particles and large particles, respectively.

Fig 7 3-Dimensional images of nanoparticles on quartz glass wafer with different experiment conditions: (A) heat treatment of Ag^+/PVA/PVP composite film with reduction[35] (sample 7); (B) heat treatment of Ag^+/PVA composite film without reduction (sample 8); (C) heat treatment of Ag^+/PVA/PVP composite film without reduction[35] (sample 1). These films are two layers.

Fig 8 TGA analysis of the Ag^+/PVA/PVP composite film. The mole ratio of PVA, PVP and $AgNO_3$ is 4:1:4.

RSC Advances Accepted Manuscript

Fig 9 SERS spectra of 4-ATP (1×10^{-6} M) on Ag nanoparticles film prepared with different experiment conditions. Black, red and blue lines correspond to the sample 1, sample 7 and sample 8, respectively.

Fig 10 SERS spectra of R6G (1×10^{-6} M) on Ag nanoparticles film prepared with different experiment conditions. Black, red and blue lines correspond to the sample 1, sample 7 and sample 8, respectively.

Fig 11 E-field amplitude patterns from theoretical calculations at the excitation wavelength of 514.5 nm for (A-C) Ag nanoring attached one small Ag nanoparticle with exterior surface; (D-F) Ag nanoring attached one small Ag nanoparticle with interior surface. The diameter of small Ag nanoparticle is 20 nm. The arrows represent the different polarization directions: (A, C) 0°, (B, E) 45°, and (C, F) 90°.

Fig 12 E-field amplitude patterns from theoretical calculations at the excitation wavelength of 514.5 nm for Ag nanoring attached one different diameter small Ag nanoparticle with exterior surface: (A) 10 nm, (B) 15 nm, (C) 25 nm, (D) 30 nm.

RSC Advances Accepted Manuscript

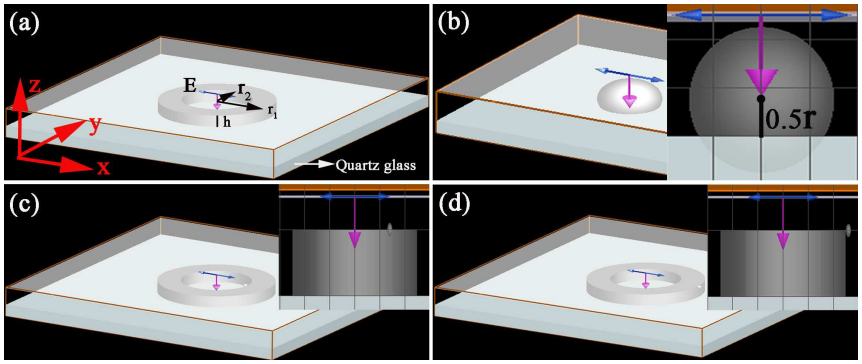

Fig. 1

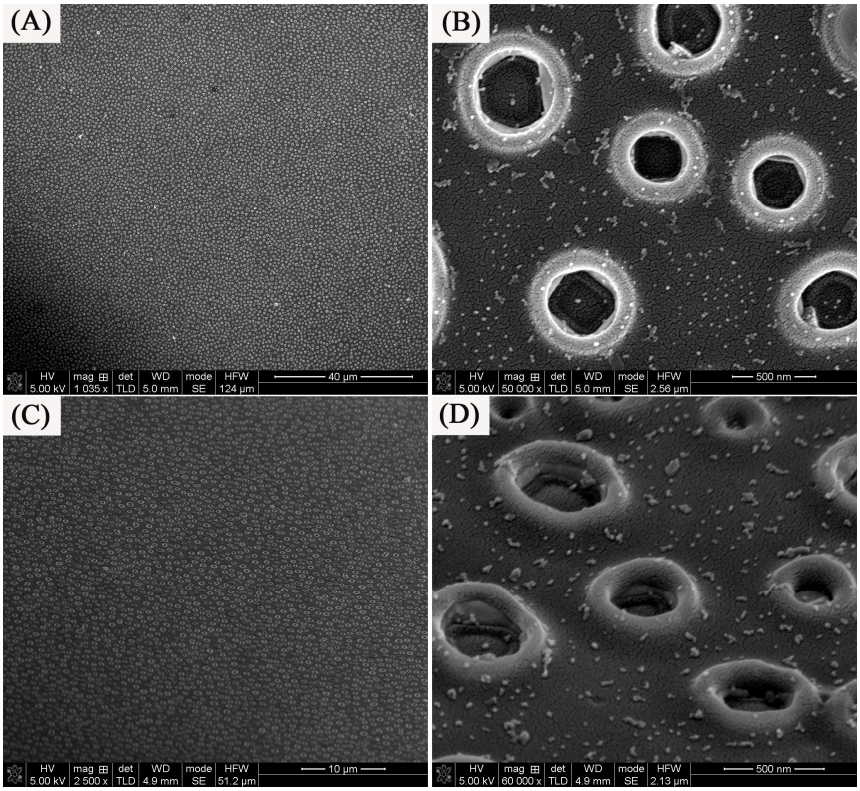

Fig. 2

RSC Advances Accepted Manuscript

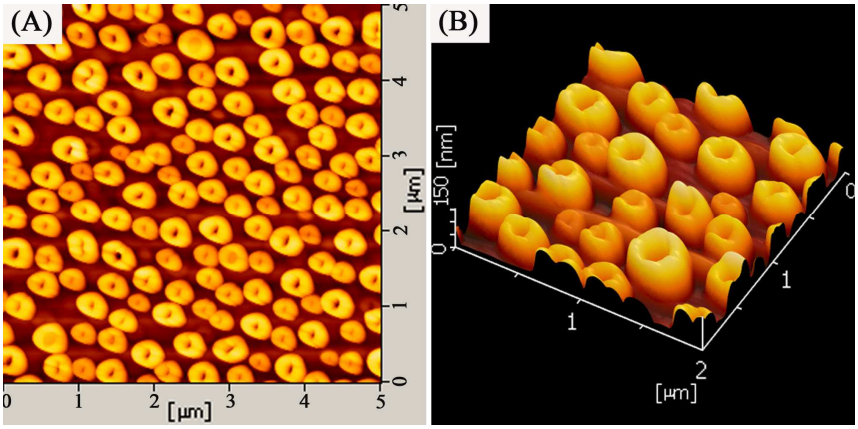

Fig. 3

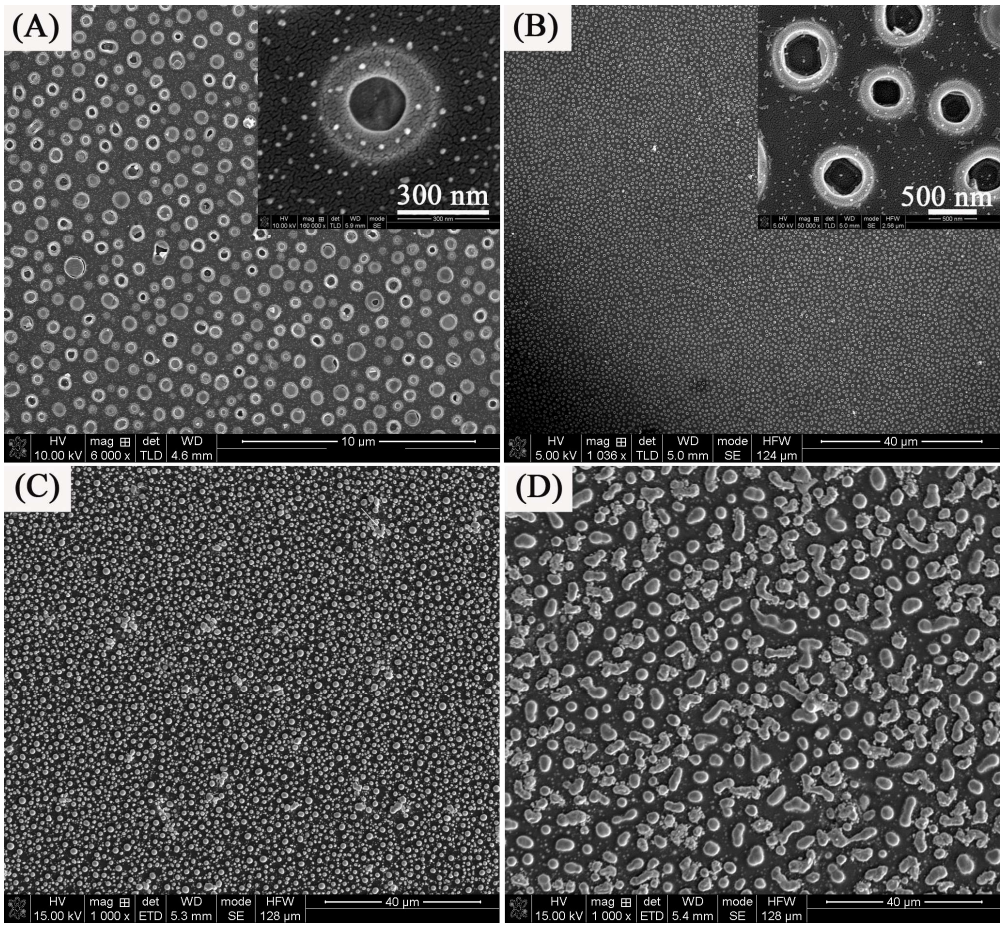

Fig. 4

RSC Advances Accepted Manuscript

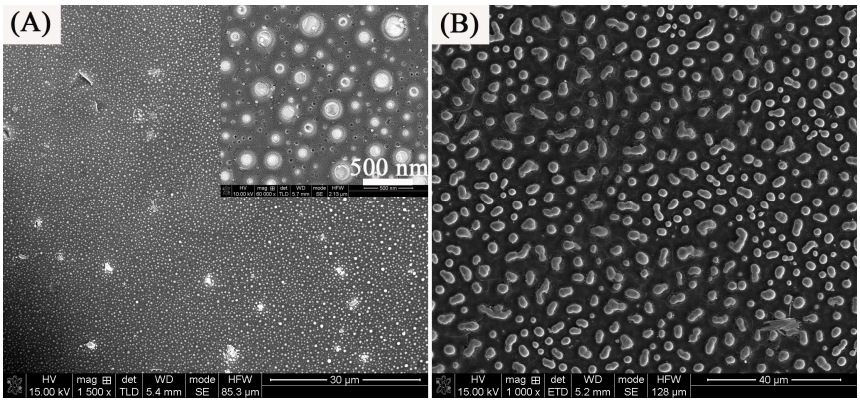

Fig. 5

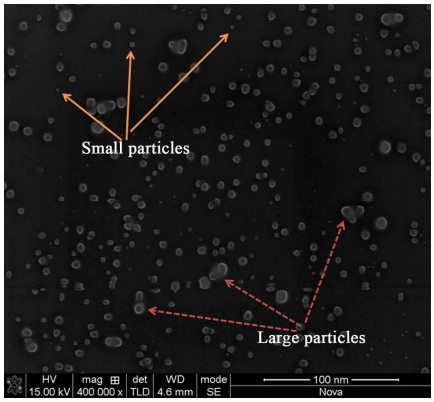

Fig. 6

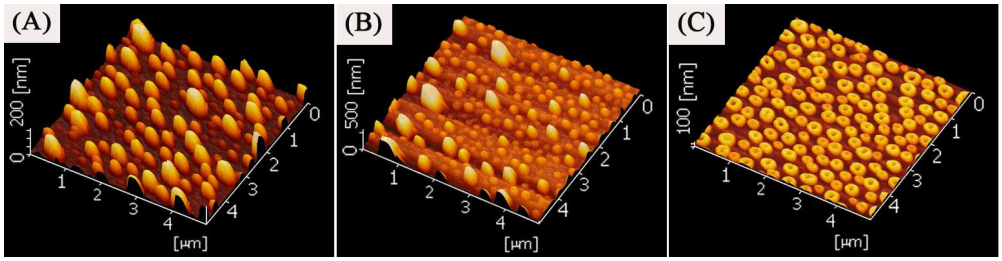

Fig. 7

RSC Advances Accepted Manuscript

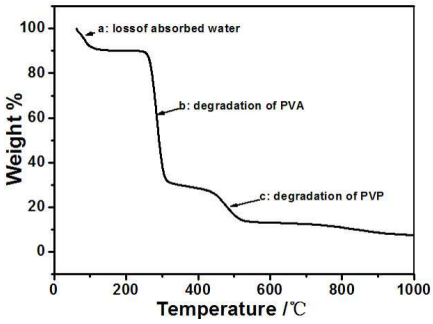

Fig. 8

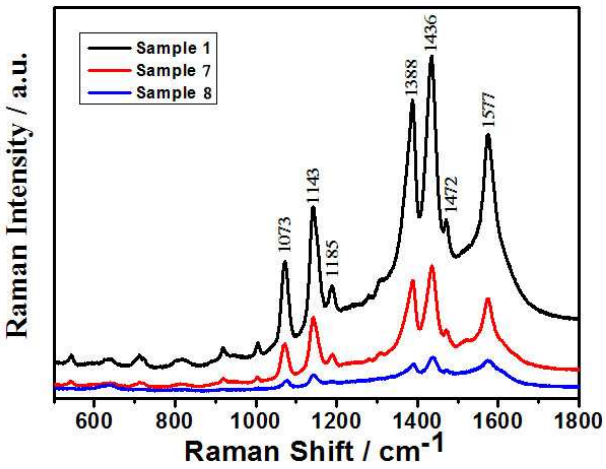

Fig. 9

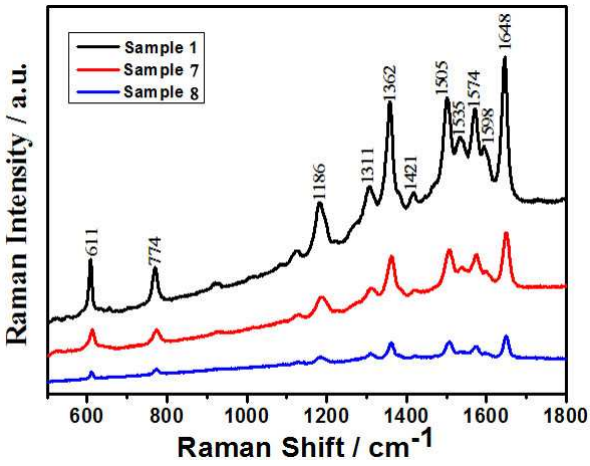

Fig. 10

RSC Advances Accepted Manuscript

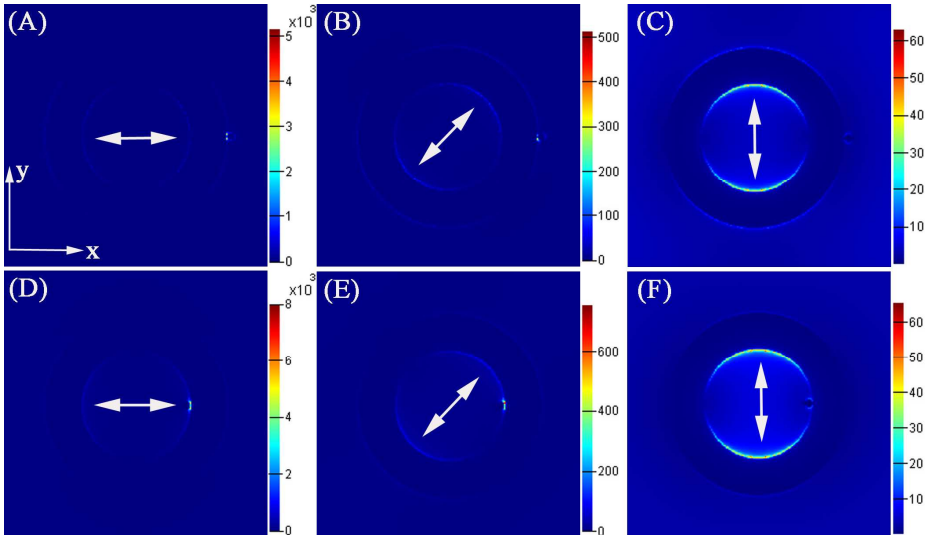

Fig. 11

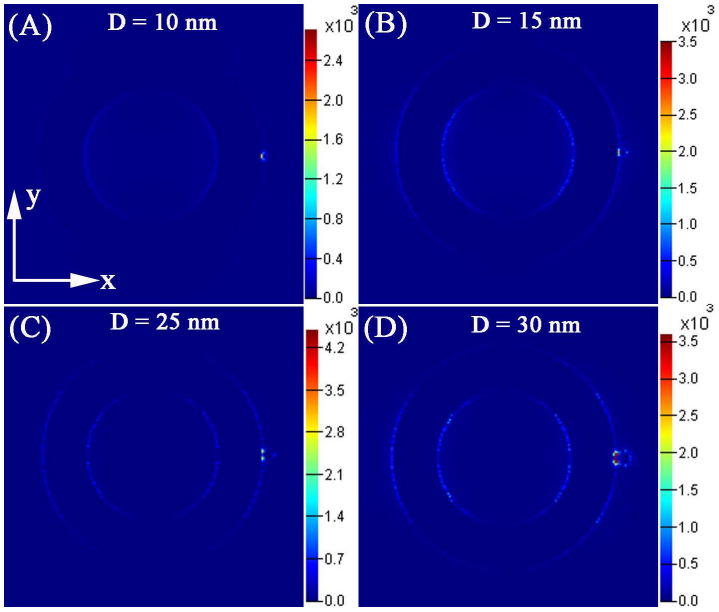

Fig. 12

RSC Advances Accepted Manuscript